Time-dependent gas density and temperature measurements in pulsed helicon discharges in argon

INSTITUTE OF PHYSICS PUBLISHING PLASMA SOURCES SCIENCE AND TECHNOLOGY
Plasma Sources Sci. Technol. **12** (2003) 345–357 PII: S0963-0252(03)62646-0

Time-dependent gas density and temperature measurements in pulsed helicon discharges in argon

B Clarenbach[1], **B Lorenz**[1], **M Krämer**[1] **and N Sadeghi**[2]

[1] Experimentalphysik II, Ruhr-Universität Bochum, D-44780 Bochum, Germany
[2] Laboratoire de Spectrométrie Physique, Université Joseph Fourier—Grenoble I and CNRS, B.P. 87 38402 Saint Martin d'Hères Cedex, France

E-mail: mk@ep2.rub.de

Received 5 November 2002, in final form 23 April 2003
Published 22 May 2003
Online at stacks.iop.org/PSST/12/345

Abstract
Time-dependent measurements of the temperature and density of the $Ar^*(^3P_0)$ metastable atoms in two high-density pulsed helicon discharges, deduced from the absorption profile of the 772.42 nm argon line, are presented. A single-mode tuneable diode laser is used for recording these profiles, and temperatures up to 1000 K are obtained from their Doppler width. As in high-density plasmas the metastable and ground-state atoms are strongly coupled by electron impact collisions, the temperature of the metastable atoms reflects the gas temperature. From the time variation of the $Ar^*(^3P_0)$ density during the discharge pulse we were able to deduce the density of the ground-state argon atoms and found for the helicon regime that the neutral atoms can be depleted by more than a factor of 10. Over a wide range of plasma parameters, we examined the axial asymmetry that is characteristic for helicon discharges with helical antenna coupling. In particular, we analysed the plasma-induced emission of the Ar (750 nm) and Ar^+ (461 nm) lines as well as the electron density in the beginning of the plasma pulse to better understand the evolution of the plasma and the transition to the helicon regime. The measurements of the gas temperature and the metastable density reveal the asymmetry to become pronounced when the discharge changes from inductively coupled plasma to the helicon discharge. In the helicon regime, the argon atom depletion of up to 90% and ionization degrees up to 65% were achieved in the antenna zone. In the afterglow, all excited states of argon, including the $Ar^*(^3P_0)$ state, are fed by electron–Ar^+ ion recombination. The measured very high temperature of $Ar^*(^3P_0)$ atoms is partially related to the temperature of the Ar^+ ions. Production of Ar^+ in its excited states is also observed during several hundreds of microseconds in the afterglow. It is related to the electron–Ar^{2+} ion recombination and indicates the presence of a significant amount of doubly charged argon ions in the present helicon plasmas.

1. Introduction

Helicon discharges are produced and sustained by helicon modes that are whistler waves travelling in a magnetized plasma column, i.e. in bounded plasma [1, 2]. These high-density sources operate typically at frequencies between the lower hybrid and the electron cyclotron frequency. To launch the *rf* power into the plasma various antennas have been used. The distribution of the *rf* current flowing in the coupling antenna is crucial for the *rf* power deposition and, thus, the spatial distribution of the plasma parameters depends on the particular antenna geometry. In case of helical antennas, a

pronounced axial asymmetry with respect to the centre of the antenna may be observed, which can be attributed to the different propagation behaviours of the helicon modes [3–6]. If the *rf* power is coupled to the plasma column via a right-handed helical Shoji-type antenna [7], helicon modes with the azimuthal mode number $m = +1$ propagate on one side of the antenna and $m = -1$ on the other side, depending on the direction of the magnetic field. However, in most cases, the $m = +1$ mode carries the major fraction of the *rf* power so that the *rf* power is deposited preferably on the corresponding side of the antenna. In the following, we denote this side, where the electron density is higher, as the $m = +1$ side of the antenna and the other as the $m = -1$ side.

In this paper, we have measured the time-dependent electron and argon metastable densities on two highly ionized pulsed helicon discharges in argon. The emission intensities of several atomic and ionic lines have also been analysed. Our data enable us to deduce, for the first time, the variation of the gas temperature T_g in a wide range of parameters during the *rf* pulse as well as in the afterglow. T_g was obtained from the evolution of the Doppler profile of the 772.42 nm ($2p_2 \leftarrow {}^3P_0$) absorption line. In the present helicon discharges with electron densities $n_e > 10^{18}\,m^{-3}$ and a temperature $T_e \cong 3\,eV$, the $Ar^*({}^3P_0)$ metastable atoms are produced by direct electron impact excitation of the ground-state atoms, or through the higher lying excited states after radiative cascades. Under these conditions, the main destruction mechanism of the $Ar^*({}^3P_0)$ atoms is by collisions with electrons. They include transfer to the adjacent resonance state $Ar^*({}^1P_1)$,

$$Ar^*({}^3P_0) + e \rightarrow Ar^*({}^1P_1) + e, \qquad (1)$$

followed by the emission of 104 nm radiation to the ground-state as well as ionization, excitation to the higher 4p states and transfers to the $Ar^*({}^3P_1)$ and $Ar^*({}^3P_2)$ states. We should point out that even in discharges with very low electron temperature, the reported relative populations of $Ar^*({}^3P_2)$ and $Ar^*({}^3P_0)$ metastable states are often very close to the ratio of their statistical weights $\frac{5}{1}$ [8]. It is obvious that in helicon discharges, the equilibrium condition by electron collision transfer between states is fully satisfied. Therefore, at any time, the $Ar^*({}^3P_0)$ density is representative of the total metastable density in the plasma.

The total electron impact quenching rate coefficient of $Ar^*({}^3P_2)$ metastable atoms, k_q, was measured as $2 \times 10^{-13}\,m^3\,s^{-1}$ for $T_e > 0.3\,eV$ [9, 10], and we expect a similar rate coefficient for reaction (1), even if a coefficient three times larger has been proposed in [11]. For electron densities $n_e > 5 \times 10^{17}\,m^{-3}$ considered in this paper, the lifetime of the monitored $Ar^*({}^3P_0)$ metastable atoms is therefore short enough ($<10\,\mu s$) to preserve their velocity distribution, i.e. that of the ground-state argon atoms, when they are produced. Moreover, the cross-section for metastability exchange, σ_{mx}, through collisions between metastable and ground-state atoms is about $1 \times 10^{-18}\,m^2$ [3]. These atoms exchange momentum at a rate frequency of about $1 \times 10^5\,s^{-1}$. Therefore, the temperature deduced from our measurements corresponds to the temperature T_g of the neutral atoms.

The results presented in this paper also give information on the variation of the neutral gas density n_g during the plasma pulse. Knowledge of T_g and n_g enables us to estimate more accurately the different collisional and collisionless *rf* absorption processes in the plasma. Moreover, they are indispensable quantities for a proper self-consistent description of helicon discharges as well as for the evaluation of emission spectroscopic measurements with the aid of a collisional-radiative model for argon. As helicon discharges have high electron density and low gas pressure, the dominant processes are electron impact excitation and de-excitation, ionization and radiative decay; metastable diffusion to the wall and their de-excitation in collisions with argon atoms [12, 14] can be neglected.

This paper is arranged as follows. In section 2, we describe the experimental set-up and, in particular, the principles of the absorption measurements. The experimental results are presented and interpreted in section 3. First, we describe the formation of the helicon discharge discussing, in particular, the asymmetry of the discharge and the electron heating mechanism. In the following sections, we deal with the density evolution of the metastable argon atoms, the neutral gas atoms and the electrons during the *rf* pulse; we also describe the temporal behaviour of the metastable atoms in the afterglow. Finally, section 4 contains conclusions.

2. Experiment

The measurements were carried out on two pulsed helicon wave discharges operating in argon, the high-density discharge HE-S with small diameter shown in figure 1 ($r_p = 2.8\,cm$, $L_p = 1.4\,m$) and the large-volume helicon source HE-L ($r_p = 7.8\,cm$, $L_p = 2\,m$) [5, 6]. The plasma was produced by *rf* power pulses ($P_{rf} \leqslant 2\,kW$, $\tau_{pulse} = 2\,ms$, $f_{pulse} = 25\,Hz$) through helical antennas surrounding the discharge tube (quartz). The coupling antenna used on HE-S is essentially a twisted double-saddle coil consisting of two pairs of helical windings with opposite direction of the *rf* current and 180° pitch over the antenna length $L_a = 11\,cm$. Figure 2 shows a schematic of the antenna where, for simplicity, the *rf* power input connectors have been omitted. In practice, the two current circuits are in series forming one circuit (see [15]). On HE-L, we used a (Shoji-type [7]) helical antenna of length $L_a = 22\,cm$. The particular geometry of both antennas provides $m = +1$ ($m = -1$) helicon mode excitation in positive (negative) magnetic field direction. The experimental parameters are typically $n_e \leqslant 6 \times 10^{19}\,m^{-3}$, $T_e \approx 3\,eV$, $f_{rf} = 25\,MHz$, $p = 0.5$–$3\,Pa$ and $B_0 \leqslant 0.16\,T$ for HE-S, while in HE-L the electron density is a factor of five smaller, and the remaining parameters are $T_e \approx 3\,eV$, $f_{rf} = 13.56\,MHz$, $p = 0.1$–$2\,Pa$ and $B_0 \leqslant 0.1\,T$. In this paper, we mostly present data from the HE-S discharge, but comparable results have also been obtained on the HE-L device.

The temperature and the mean density of the metastable $Ar^*({}^3P_0)$ atoms (also identified as $1s_3$ in Paschen and $4s'[1/2]^0$ in Racah notations, respectively [16]) were deduced from

[3] σ_{mx} is deduced from the diffusion coefficient of argon metastable atoms in argon, $D = 1.7 \times 10^{20}\,molecule\,m^{-1}\,s^{-1}$ at 300 K [12], given by $D = (3\pi/16\sqrt{2})\langle w\rangle/\sigma$, where $\langle w\rangle$ is the mean velocity of argon atoms at 300 K [13].

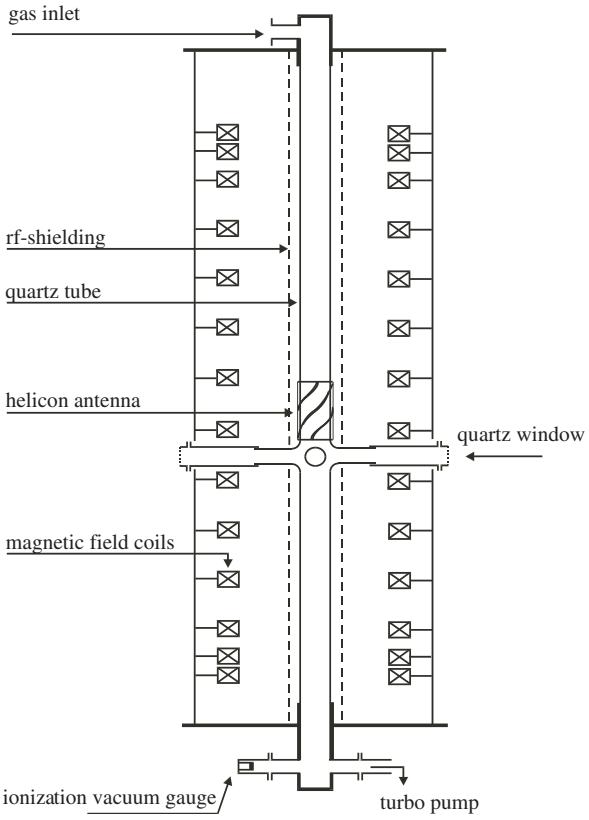

Figure 1. Experimental set-up of the HE-S helicon discharge.

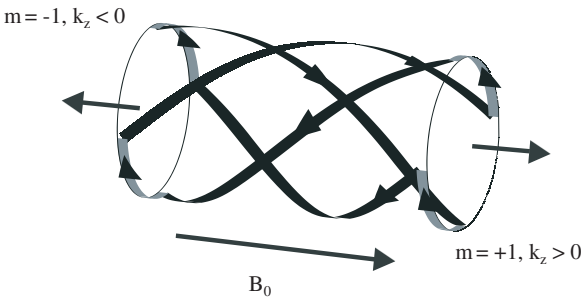

Figure 2. Helicon antenna on the HE-S helicon discharge.

absorption spectroscopy measurements by means of a single-mode diode laser scanning the 772.42 nm ($2p_2 \leftarrow {}^3P_0$) line. Figure 3 shows a schematic of the experimental set-up. After being sufficiently attenuated to avoid saturation and optical pumping [17], the laser beam crosses the plasma tube transversely, 5 and 43 cm apart from the ends of the helical antennas on the HE-S and HE-L discharges, respectively. To double the absorption length and increase the sensitivity, the beam is reflected by a mirror and then detected with a photomultiplier (PMT). A 2 mm diameter iris and a high-pass IR filter are placed in front of the PMT to minimize the plasma emission signal. The signal of the PMT is acquired by a digital oscilloscope, triggered synchronously with the *rf* pulse that produces the plasma; the time resolution of the system (given by the input resistance of the amplifier following the PMT) is about 1 μs while a sample rate of 10 μs was chosen in our absorption measurements.

The polarization of the laser light was chosen parallel to the external magnetic field to provide absorption on only one π ($m = 0 - m = 0$) Zeeman component of the line (J values of the lower and upper states are 0 and 1, respectively). The laser frequency was varied in steps of 0.06 GHz and at each frequency the PMT signal was averaged over 128 plasma pulses and then recorded in a file. Similarly, we measured and processed the time-dependent emission signal when the laser beam is blocked, and subtracted the corresponding file from the absorption files. In this way, we obtain the waveforms of the transmitted laser signal for about 40 laser frequency components forming the absorption line profile. For each frequency, the signal in the corresponding file is converted to the line-averaged time-dependent metastable density, $\langle N(\nu, t)\rangle$, using the relation [18]

$$\ln\left(\frac{I_0}{I_\nu(\nu,t)}\right) = \frac{1}{4\pi\varepsilon_0}\frac{\pi e^2}{m_e c} l f \langle N(\nu,t)\rangle g(\nu,t), \qquad (2)$$

where I_0 is the signal without absorption (i.e. before the plasma pulse), $l = 2 \times 2r_p$ is the absorption path length, $f = 0.341$ is the oscillator strength of the transition [16] and $g(\nu, t)$ is the normalized line profile, $\int_{-\infty}^{+\infty} g(\nu,t)\,\mathrm{d}\nu = 1$, related to the distribution function of the velocity of atoms along the laser beam. Figure 4 shows an example of the contour plot of $\langle N(\nu, t)\rangle$ obtained from data recorded at different frequencies. Assuming the velocity distribution function to be a Gaussian, the profile can be written as

$$g(\nu,t) = \frac{2}{\gamma_D(t)}\sqrt{\frac{\ln 2}{\pi}}\exp\left(-4\ln 2\left(\frac{\Delta\nu}{\gamma_D(t)}\right)^2\right), \qquad (3)$$

where $\gamma_D(t) = (2\sqrt{\ln 2}/\lambda_0)\sqrt{k_B T(t)/M}$ is the Doppler width (FWHM) related to the time-dependent temperature $T(t)$ of the metastable atoms and $\Delta\nu$ is the frequency shift from the line centre. Therefore, the line-averaged translational temperature, $T(t)$ can be deduced from the profile of the section at any time t of the three-dimensional-plot in figure 4 and the metastable density, $\langle N(t)\rangle$ from the integral over the laser frequency of this profile. Figure 5 shows two examples of the metastable density profiles taken 0.1 and 1.88 ms after the breakdown of the plasma. We obtained $T(t)$ by fitting the line profile to a Gaussian and $\langle N(t)\rangle$ by integrating over the profile.

To analyse the influence of the electron density n_e on $\langle N(t)\rangle$ and $T(t)$, we used a Langmuir probe measuring the time-dependent ion saturation current that is proportional to n_e. The absolute density was then obtained by calibration with a microwave interferometer ($\lambda = 4$ mm on HE-S, $\lambda = 8$ mm on HE-L).

On the HE-S discharge, we also recorded the time-dependent emission intensity of several argon lines during the *rf* pulse and in the afterglow by means of a 25 cm monochromator (Jarrel-Ash Ebert optical mount) backed by a PMT. A quartz lens and a mirror provide the image of the plasma zone on the entrance slit of the monochromator monitored by laser absorption. The emission signal is averaged and acquired by a digital oscilloscope with a time resolution of 10 μs. The observed lines correspond to the infrared 4p $\rightarrow$ 4s transitions of the argon atom and the 461 nm line of the Ar^+ ion.

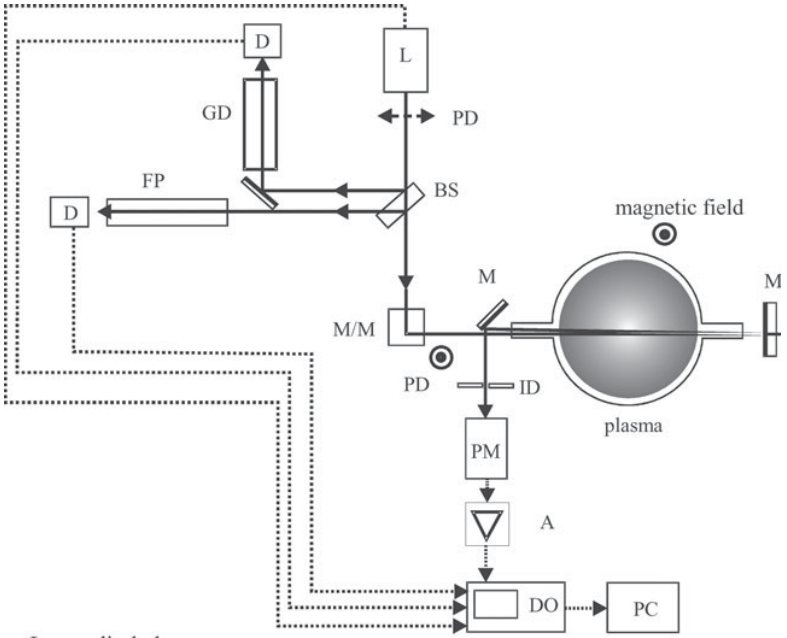

L : diode laser
DP : polarization direction
BS : beam splitter
M : mirror
M/M: two mirrors, rotate the direction of polarization of the laser through 90°
ID : iris diaphragm
D : detector
FP : Fabry-Perot interferometer
GD : glow discharge (Ar)
PM : photomultiplier
DO : digital storage oscilloscope
A : dc amplifier
PC : computer

Figure 3. Schematic diagram for the absorption measurements.

3. Experimental results

The density and the temperature of the $Ar^*(^3P_0)$ metastable atoms were measured for different plasma parameters, namely, the gas pressure, the *rf* power and the magnetic field strength. By changing the direction of the external magnetic field, we were able to monitor both sides of the antenna and, thus, to study the axial asymmetry of the helicon discharge which is intimately related to the different propagation behaviours of the $m = +1$ and $m = -1$ helicon modes.

As an example, figure 6 shows the time-dependence of the gas temperature and the metastable density for both magnetic field directions measured on the HE-S discharge at $p = 1$ Pa, $B_0 = 0.1$ T and $P_{rf} = 1.4$ kW; in figure 6(*b*) we also plotted the electron density n_e. Note that the T_g values of figure 6(*a*) are deduced from the velocity distribution function of $Ar^*(^3P_0)$ atoms averaged along the plasma diameter. A question to be answered is whether this velocity distribution is not affected by a possible drift velocity of metastable atoms toward the wall. However, these neutral atoms cannot be accelerated by a radial electric field to gain directed velocity. On the other hand, as the quenching rate coefficient of metastable atoms, k_q, is very large, due to the high electron densities (in the order of 10^{19} m^{-3}), the mean free path of $Ar^*(^3P_0)$ atoms is about 1 mm and, thus, much shorter than the plasma diameter. Therefore, the metastable and ground-state atoms are in thermodynamic equilibrium and, assuming no radial drift of the ground-state atoms, we conclude that the temperature shown in figure 6(*a*) corresponds to that of the neutral atoms in the plasma.

In figure 6(*b*), immediately after beginning the plasma pulse, the metastable density increases up to its maximum value after about 0.1 ms. After that, it decreases rapidly by almost one order of magnitude at about 0.5 ms and then remains practically constant until the end of the pulse. In the following section we will explain that this drop is closely related to the gas depletion due to the simultaneous action of the rise of the gas temperature at constant pressure, the ionization of the argon neutrals, and the ion drag. At the end of the discharge pulse, the metastable density drops very rapidly, while the electron density decreases much more slowly. The very fast loss of energetic electrons stopping the production of $Ar^*(^3P_0)$ atoms, and the continuation of their efficient quenching by bulk electrons, is responsible

DOCKET ALARM

Explore Litigation Insights

Docket Alarm provides insights to develop a more informed litigation strategy and the peace of mind of knowing you're on top of things.

Real-Time Litigation Alerts

Keep your litigation team up-to-date with **real-time alerts** and advanced team management tools built for the enterprise, all while greatly reducing PACER spend.

Our comprehensive service means we can handle Federal, State, and Administrative courts across the country.

Advanced Docket Research

With over 230 million records, Docket Alarm's cloud-native docket research platform finds what other services can't. Coverage includes Federal, State, plus PTAB, TTAB, ITC and NLRB decisions, all in one place.

Identify arguments that have been successful in the past with full text, pinpoint searching. Link to case law cited within any court document via Fastcase.

Analytics At Your Fingertips

Learn what happened the last time a particular judge, opposing counsel or company faced cases similar to yours.

Advanced out-of-the-box PTAB and TTAB analytics are always at your fingertips.

API

Docket Alarm offers a powerful API (application programming interface) to developers that want to integrate case filings into their apps.

LAW FIRMS
Build custom dashboards for your attorneys and clients with live data direct from the court.

Automate many repetitive legal tasks like conflict checks, document management, and marketing.

FINANCIAL INSTITUTIONS
Litigation and bankruptcy checks for companies and debtors.

E-DISCOVERY AND LEGAL VENDORS
Sync your system to PACER to automate legal marketing.